Sensor domain of histidine kinase KinB of Pseudomonas: a helix-swapped dimer

Article *in* Journal of Biological Chemistry · February 2014

DOI: 10.1074/jbc.M113.514836 · Source: PubMed

Protein Structure and Folding:

Sensor Domain of Histidine Kinase KinB of *Pseudomonas*: A HELIX-SWAPPED DIMER

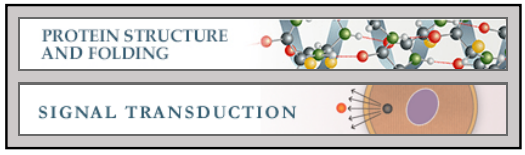

Kemin Tan, Gekleng Chhor, T. Andrew Binkowski, Robert P. Jedrzejczak, Magdalena Makowska-Grzyska and Andrzej Joachimiak

J. Biol. Chem. 2014, 289:12232-12244.
doi: 10.1074/jbc.M113.514836 originally published online February 26, 2014

THE JOURNAL OF BIOLOGICAL CHEMISTRY VOL. 289, NO. 18, pp. 12232–12244, May 2, 2014
Published in the U.S.A.

Sensor Domain of Histidine Kinase KinB of *Pseudomonas*

*A HELIX-SWAPPED DIMER**

Received for publication, September 9, 2013, and in revised form, February 20, 2014 Published, JBC Papers in Press, February 26, 2014, DOI 10.1074/jbc.M113.514836

Kemin Tan[‡§¶], Gekleng Chhor[‡], T. Andrew Binkowski[‡], Robert P. Jedrzejczak[‡], Magdalena Makowska-Grzyska[¶1], and Andrzej Joachimiak[‡§¶2]

From the [‡]Midwest Center for Structural Genomics and [§]Structural Biology Center, Biosciences, Argonne National Laboratory, Argonne, Illinois 60439 and the [¶]Center for Structural Genomics of Infectious Diseases, University of Chicago, Chicago, Illinois 60637

Background: The sensor domain (SD) of histidine kinase (HK) KinB (KinB-SD) receives signals from the environment and induces a transduction cascade.
Results: Structures of the KinB-SD were obtained in ligand-free, phosphate-bound, and mutant forms.
Conclusion: The unique helix-swapped KinB-SD structure forms a ligand-binding cavity on the dimer interface.
Significance: KinB-SD studies provide insights into the signal transduction and identity of potential signaling molecules.

The overproduction of polysaccharide alginate is responsible for the formation of mucus in the lungs of cystic fibrosis patients. Histidine kinase KinB of the KinB-AlgB two-component system in *Pseudomonas aeruginosa* acts as a negative regulator of alginate biosynthesis. The modular architecture of KinB is similar to other histidine kinases. However, its periplasmic signal sensor domain is unique and is found only in the *Pseudomonas* genus. Here, we present the first crystal structures of the KinB sensor domain. The domain is a dimer in solution, and in the crystal it shows an atypical dimer of a helix-swapped four-helix bundle. A positively charged cavity is formed on the dimer interface and involves several strictly conserved residues, including Arg-60. A phosphate anion is bound asymmetrically in one of the structures. *In silico* docking identified several monophosphorylated sugars, including β-D-fructose 6-phosphate and β-D-mannose 6-phosphate, a precursor and an intermediate of alginate synthesis, respectively, as potential KinB ligands. Ligand binding was confirmed experimentally. Conformational transition from a symmetric to an asymmetric structure and decreasing dimer stability caused by ligand binding may be a part of the signal transduction mechanism of the KinB-AlgB two-component system.

Overproduction of the exopolysaccharide alginate by *Pseudomonas aeruginosa* in bacterial pulmonary infections leads to the buildup of mucus in the lungs of patients with cystic fibrosis (1). Alginate biosynthesis is tightly controlled by a set of genes and a cascade of regulators (2–4). One of these is AlgB, which was shown to serve as a negative regulator of alginate production (5). AlgB is a two-component response regulator of the NtrC family (6). The cognate sensor kinase of AlgB is KinB (GI:15600677), which is a histidine kinase (HK)[3] (7).

Similar to many HKs, KinB, at its N terminus, has a periplasmic sensor domain (KinB-SD) (~120 amino acids) flanked by two transmembrane helices that anchor it to the membrane (7). The sensor domain (SD) is unique to the *Pseudomonas* genus and has no significant sequence similarity with any other known proteins. Within the different strains of *P. aeruginosa*, the sequence identities are larger than 85%. The sequence identity with other members of the *Pseudomonas* genus is between 28 and 35%. After the second transmembrane helix, the cytoplasmic portion of KinB is a regular HK that is composed of several domains as follows: (i) a histidine kinases, adenyl cyclases, methyl-accepting proteins, and phosphatases (HAMP) domain; (ii) Per-Arnt-Sim (PAS) domain, and (iii) a His-kinase-A (phosphoacceptor) core containing a specific histidine-containing dimerization subdomain and a kinase subdomain. In alginate regulation, it is believed that the KinB-AlgB (HK-RR) pair works similarly to other two-component systems (TCSs) in signal relay from the periplasm to cytoplasm, such as the PhoQ-PhoP and PmrB-PmrA pairs among others found in *P. aeruginosa* (8). A typical TCS signaling mechanism involves the periplasmic KinB-SD receiving an environmental signal. Binding a signal molecule causes a structural change in the SD that is transmitted across the membrane resulting in the autophosphorylation of the specific histidine in the dimerization subdomain of the HK core. The phosphate is then transferred to a specific aspartate of the response regulator, AlgB. Subsequently, AlgB mediates AlgW-dependent MucA proteolysis leading to the reduction of alginate biosynthesis (5). Recent studies have significantly expanded the function of KinB. It was

* This work was supported, in whole or in part, by National Institutes of Health Grants GM074942 and GM094585. This work was also supported by United States Department of Energy, Office of Biological and Environmental Research, Contract DE-AC02-06CH11357. This article was created by UChicago Argonne, LLC, Operator of Argonne National Laboratory ("Argonne"). Argonne, a United States Department of Energy Office of Science laboratory, is operated under Contract DE-AC02-06CH11357.
The atomic coordinates and structure factors (codes 3KKB, 3L34, 4LLE, and 4LLC) have been deposited in the Protein Data Bank (http://wwpdb.org/).
[1] Supported by National Institutes of Health Grants HHSN272200700058C and HHSN272201200026C.
[2] To whom correspondence should be addressed. E-mail: andrzejj@anl.gov.

[3] The abbreviations used are: HK, histidine kinase; SD, sensor domain; TCS, two-component system; Man-6-P, β-D-mannose 6-phosphate; Fru-6-P, β-D-fructose 6-phosphate; SeMet, seleno-methionine; r.m.s.d., root mean square deviation; BLI, biolayer interferometry; DSF, differential scanning fluorimetry; DLS, dynamic light scattering; PDB, Protein Data Bank; PAS, Per-Arnt-Sim; SAD, single-wavelength anomalous diffraction; LS, least squares.

shown that in addition to alginate synthesis down-regulation, KinB seems to control a large number of genes coding for virulence factors that are important to the development of acute pneumonia and causes a switch between chronic and acute infection (9, 10). KinB also appears to be essential in acute infections in zebrafish embryos and other virulence-associated phenotypes, such as quorum sensing, biofilm formation, and motility (11). These phenotypes, however, are independent of KinB's kinase activity and its response regulator AlgB, indicating an atypical, noncanonical TCS signaling mechanism (10). Moreover, one report suggested that in the regulation of virulence, KinB functions as a phosphatase to dephosphorylate AlgB instead of an AlgB kinase (12). It is not clear whether these KinB functions involve signaling molecule(s). All of these data added complexity to the regulatory activities of KinB and the signal transduction pathways. It is believed that a part of the intricacy may involve possible diverse responses of SDs to different signaling molecules. Despite these recent discoveries, the KinB-SD and its signaling molecule(s) have remained uncharacterized. Understanding the KinB signal transduction mechanism and identifying the signaling molecules may be important for developing cystic fibrosis treatments.

The HK SDs of TCSs have been investigated previously (13–15). These domains show significant sequence diversity, and it is believed that they can recognize a wide variety of chemical signals. Upon binding a ligand, the information is transmitted into the cell, initiating a kinase response. The majority of previously characterized SDs adopt two main types of structural scaffolds, the PAS-like and four-helix bundle domains. A PAS-like (16) or "PDC" fold (17) is represented by the structures of PhoQ (17, 18), DcuS (19), and CitA (16). The double PAS-like domain has also been observed in LuxQ (20), DctB (21, 22), and in recently reported KinD (23). PAS-like SDs are believed to serve as ligand recognition units in extracytoplasmic signal transduction proteins (24). A four-helix bundle SD is represented by NarX (25), and a double four-helix bundle SD is represented by TorS (26). This domain is believed to be a ubiquitous sensor module for HKs, and it contributes conserved residues to the dimerization interface (27). In both PAS-like and four-helix bundle SDs, a conformational change in the dimer upon signaling molecule binding is recognized as a necessary and key step in the signal transduction from the periplasmic to the cytoplasmic portion of TCSs. Other structural scaffolds for HK have also been observed. Hendrickson and co-workers (28) reported a functionally uncharacterized SD ($HK29_s$) of HK encoded by the *Geobacter sulfurreducens* GSU2755 gene. $HK29_s$ shows a periplasmic solute-binding protein fold described as a "Venus flytrap" (28). A double periplasmic solute-binding protein sensor domain has also been identified and described in the sensor kinase BvgS of the TCS BvgAS (29), which regulates the virulence of *Bordetella pertussis* in whooping cough (30). Recently, crystal structures of a SD consisting of two seven-blade β-propellers and an Ig-like fold have also been reported from a *Bacteroides thetaiotaomicron* hybrid TCS, which contains all the domains of a typical HK in a single polypeptide (31). The discovery of a periplasmic solute-binding protein, a seven-blade β-propeller, and an Ig-like SD expands the structural modules used for signaling in TCSs and shows a more diverse set of signaling molecule receptors associated with HKs.

Some SDs are found across many species and super-kingdoms, but some are unique to a specific genus. *Pseudomonas* KinB-SDs belong to the latter group and show a unique sequence. A secondary structure prediction suggests an all-helical structure placing it in a four-helix bundle subgroup. However, the conserved residues found in four-helix bundle SDs are not present (27). Initially, KinB was aligned and compared with a SD of HK PhoR from *Bacillus subtilis,* with which it shares 31% amino acid sequence identity and 59% similarity (7). A recently reported PhoR SD structure revealed an α/β PAS-like fold (24).

Here, we present high resolution crystal structures of the KinB-SD in a ligand-free form and a complex with a bound phosphate. These structures reveal an all-helical four-helix bundle structure, consistent with secondary structure predictions, forming an atypical helix-swapped dimer. Interestingly, KinB sequence similarity to PhoR suggests that PAS-like SDs may be evolutionally related. Several site-directed mutations were introduced to confirm helix swapping, and structures of R60L and R60E mutants were determined. Inspired by the unique cavity formed on the interface between two monomers where the phosphate group was found, *in silico* ligand screening was performed. Among the top scoring ligands were several monophosphorylated sugars, including β-D-fructose 6-phosphate (Fru-6-P) and β-D-mannose 6-phosphate (Man-6-P), a precursor and an intermediate of alginate synthesis, respectively (32). Several assays were performed to evaluate ligand binding and the potential impact on KinB and its structure and function. The combination of the structural, mutagenesis, computational, and biophysical data provides clues to potential signaling molecule(s) of the KinB and a possible signal transduction mechanism.

EXPERIMENTAL PROCEDURES

Protein Cloning, Expression, and Purification—A portion of the *P. aeruginosa PAO1 kinB* gene (Gln-42 to Ala-168) corresponding to the periplasmic SD was cloned into the pMCSG19 vector. The gene was overexpressed in *Escherichia coli* BL21. The cells were grown at 37 °C in enriched M9 medium containing seleno-methionine (SeMet) under conditions known to inhibit methionine biosynthesis (33). The SeMet-labeled KinB-SD was purified from the *E. coli* cells using nickel-affinity chromatography (34). The protein was concentrated using an Amicon Ultra 3K centrifugal filter device (Millipore Inc.) in 20 mM HEPES, pH 8, 250 mM NaCl, and 2 mM dithiothreitol (DTT). The protein showed a final yield of about 40 mg/liter culture. Site-directed mutations of R60A, R60L, and R60E were created by the PIPE cloning method (35). The plasmid mentioned above was used as the template; primers were added to a final concentration of 0.4 μM, and mutagenesis was performed in a final volume of 50 μl using PfuUltra Hotstart PCR Master Mix (Stratagene). The procedure from the subsequent transformation of PCR products to mutant expression and purification was the same as described above for wild-type KinB-SD. Plasmids of mutated proteins were sequenced to confirm the presence of mutations.

The native avi-tagged KinB-SD utilized in a biolayer interferometry (BLI) study using an Octet RED system (*Forté*BIO) was created by cloning the same wild-type *kinB*-SD gene into the pMCSG62 vector, which contains an avi tag (36). The sequence confirmation, plasmid transformation, protein expression, and purification of the avi-tagged KinB-SD were the same as described for the native KinB-SD with the following exceptions: the cells were grown in LB containing 40 mM K_2HPO_4, and the protein was purified and concentrated in buffer containing 20 mM Tris, pH 8, 50 mM NaCl, and 2 mM DTT.

Size Exclusion Chromatography—Size exclusion chromatography of the wild-type KinB-SD was performed on a Superdex 200 10/300GL column using an ÄKTA FPLC (GE Healthcare). The column was pre-equilibrated with the crystallization buffer (20 mM HEPES, pH 8, 250 mM NaCl, 2 mM DTT) and calibrated with premixed protein standards, which included ribonuclease A (13.7 kDa), carbonic anhydrase (29 kDa), conalbumin (75 kDa), aldolase (158 kDa), ferritin (440 kDa), and blue dextran (2,000 kDa). The chromatography was carried out at room temperature with a flow rate of 0.3 ml/min using a 100-μl protein sample at a concentration of 47.5 mg/ml. The subsequent size exclusion chromatography of wild-type KinB and point mutants (R60A, R60L, and R60E) was performed on an SRT SEC-150 column (Sepax Technologies) connected to a Dionex HPLC equipped with a temperature-controlled autosampler housing two 96-well plate sample racks, a GP50 gradient pump, and a PDA-100 photodiode array detector (Thermo Scientific). The chromatography runs were carried out at room temperature with a flow rate of 1 ml/min. Calibration of the SRT SEC-150 column was performed with protein standards as described above.

Protein Crystallization—The proteins were screened for crystallization conditions with the help of a Mosquito nanoliter liquid handler (TTP LabTech) using the sitting drop vapor diffusion technique in 96-well CrystalQuick plates (Greiner). For each condition, 0.4 μl of protein (at 47.5 mg/ml) and 0.4 μl of crystallization formulation were mixed; the mixture was equilibrated against 140 μl of the crystallization solution in each reservoir well. The crystallization screens used were Index (Hampton Research), ANL-1 (Qiagen), and ANL-2 (Qiagen) at two temperatures, 4 and 24 °C. Diffraction quality crystals appeared under multiple conditions including the following: 1) 1.6 M sodium dihydrogen phosphate, 0.1 M phosphate-citrate, pH 4.2, and 0.4 M di-potassium hydrogen phosphate at 24 °C; 2) 0.1 M ammonium acetate, 0.1 M sodium acetate, pH 5.6, 30% PEG 4000, and 15% glycerol at 24 °C. Prior to data collection, the crystals were treated with cryoprotectants and cryocooled directly in liquid nitrogen. Co-crystallization trials with monophosphorylated sugars, including Fru-6-P and Man-6-P, were performed under crystallization condition 1 described above and supplemented with 10% of the sugars.

X-ray Diffraction and Structure Determination—A single-wavelength anomalous diffraction (SAD) data set was collected near the selenium absorption peak (12.66 keV) at 100 K from each type of KinB-SD crystal. All data were obtained at the 19-ID beamline of the Structural Biology Center at the Advanced Photon Source at Argonne National Laboratory using the program SBCcollect (37). The intensities of each data set were integrated and scaled with the HKL3000 program suite (Table 1) (38). For the phosphate-bound KinB-SD crystal containing SeMet-labeled protein, two molecules with four SeMet residues were expected in one asymmetric unit. Heavy atom sites were located using the program SHELXD (39), and four selenium sites were found and used for phasing with the program MLPHARE (40). After density modification (40), a partial model comprised of 180 residues in two chains (71% of a dimer) with 121 side chains was built in three cycles of Arp/wArp (41) model building. All of the above programs are integrated within the program suite HKL3000 (38). The model was completed manually using the program COOT (42). The final model, a helix-swapped all-helical dimer of the KinB-SD, was refined using the program Phenix.refine (Table 1) (43). The structure of the ligand-free crystal was determined using the molecular replacement method (44). The search template used was the KinB-SD swapped dimer with the connecting loops truncated. Four copies of the swapped dimers were located in the asymmetric units of the crystal. After several cycles of refinement, the connecting loops between the helices were rebuilt using $F_o - F_c$ difference electron density maps. Final refinement was carried out with the program Phenix.refine (Table 1) (43). The structure of mutant R60L was determined using the same molecular replacement approach as described for the ligand-free KinB-SD (Table 1). The structure of mutant R60E was determined using the same SeMet SAD phasing approach as described for the structure of SeMet-labeled, phosphate-bound KinB-SD (Table 1).

Differential Scanning Fluorimetry Assay—A differential scanning fluorimetry (DSF) assay was carried out using an iCycler thermal cycler (Bio-Rad) controlled by the iQ5 optical system software (Bio-Rad). The assay was performed in a 96-well PCR plate. The fluorescent dye used was SYPRO Orange (Invitrogen), which interacts with the hydrophobic portion of a protein to greatly enhance its fluorescence emission. In each well, 4 μl of 50× dye was mixed with 36 μl of protein at a concentration of 20 μM. The sample plate was sealed and centrifuged for 1 min at 1000 rpm and then placed in the thermal cycler. After 2 min, the temperature was increased gradually with a heating rate of 1 °C/min. The fluorescence intensity from each well *versus* temperature (melt curve) was measured, and a melting temperature (T_m) was calculated from the maximum value of the negative first derivative of the melt curve. The data were analyzed using GraphPad Prism Version 5.00 for Mac OS X (GraphPad Software).

Circular Dichroism Spectroscopy Assay—Circular dichroism (CD) spectroscopy was performed on a J-810 CD spectropolarimeter (Jasco). The cell path length was 1 mm, and the sensor domain protein concentration was 0.1 mg/ml with a volume of 300 μl. Each CD spectrum acquired represents an average of three scans collected from 200 to 260 nm with a step size of 0.1 nm at a rate of 50 nm/min and a bandwidth of 1 nm. For the thermal stability experiment, one spectrum was measured every 5° from 25 to 90 °C. In each step, the temperature was ramped up slowly and stabilized for 3 min before data acquisition. The baseline of each spectrum was corrected by subtracting the spectrum of a buffer blank obtained at 25 °C. The results were converted to per residue molar absorption units, $\Delta\epsilon$ (M^{-1} cm^{-1}).

TABLE 1
Data collection and crystallographic statistics

	PO_4^{2-}-bound	Ligand-free	R60L mutant	R60E mutant
Data collection				
Space group	$P3_221$	$P2_1$	$P1$	$P3_221$
Unit cell	$a = b = 75.36$, $c = 75.02$ Å	$a = 61.51$, $b = 103.08$, $c = 69.47$ Å $\beta = 90.01°$	$a = 45.23$, $b = 47.80$, $c = 49.45$ Å $\alpha = 75.98$, $\beta = 80.19$, $\gamma = 74.54°$	$a = b = 84.65$, $c = 73.9$ Å
Molecular mass (residue)	14,448 Da (130)[a]	14,448 Da (130)[a]	14,448 Da (130)[a]	14,448 Da (130)[a]
Mol (AU)	2	8	4	2
SeMet (AU)	4	16	8	4
Wavelength	0.9794 Å (peak)	0.9793 Å (peak)	0.9793 Å (peak)	0.9793 Å (peak)
Resolution	37.8 to 1.88 Å	41.4 to 1.70 Å	34.0 to 1.68 Å	36.7 to 2.00 Å
No. of unique reflections	20,202[b]	93,984[b]	42,068[b]	21,023[b]
Redundancy	5.4 (3.8)[c]	4.5 (3.8)[d]	5.0 (5.0)[e]	7.5 (7.6)[f]
Completeness	98.8% (86.3%)[c]	99.5% (94.7%)[d]	95.6% (95.9%)[e]	99.7% (100.0%)[f]
R_{merge}	9.7% (54.1%)[c]	6.8% (73.5%)[d]	6.5% (51.8%)[e]	7.6% (55.1%)[f]
$I/\sigma(I)$	23.8 (2.3)[c]	26.1 (1.5)[d]	41.0 (4.0)[e]	43.8 (3.1)[f]
Solvent content	42.2%	35.5%	28.7%	53.6%
Phasing				
R_{Cullis} (anomalous)	87%	MR[g]	MR[g]	83%
Figure of merit	20.4%[h]			15.2%[h]
Refinement				
Resolution	37.8 to 1.88	41.4 to 1.70	34.0 to 1.68	36.7 to 2.00
Reflections (work/test)	18,538/982	87,857/4875	40,952/2054	20,191/1026
$R_{crystal}/R_{free}$	16.3/22.0%	18.2/22.5%	19.6/24.2%	19.5/22.9%
r.m.s.d. from ideal geometry, Bond length/angle	0.006 Å/0.876°	0.006 Å/0.964°	0.006 Å/0.924°	0.007 Å/0.961°
No. of atoms (Protein/HETATM)	1974/223	7501/731	3700/282	1868/142
Mean B-value (Å^2) (main hain/side chain)	22.67/30.17	29.37/37.77	32.77/39.89	44.36/53.44
Ramachandran plot statistic				
Residues in most favored regions,	98.7%	96.9%	97.1%	94.5%
in additional allowed regions,	1.3%	3.1%	2.9%	5.5%
in generously allowed regions,	0%	0%	0%	0%
in disallowed region	0%	0%	0%	0%
PDB deposit	3KKB	3L34	4LLE	4LLC

[a] Data include a three-residue N-terminal tag, SNA.
[b] Data include Bijvoet pairs.
[c] The last resolution bin was 1.88–1.91 Å.
[d] The last resolution bin was 1.70–1.73 Å.
[e] The last resolution bin was 1.68–1.71 Å.
[f] The last resolution bin was 2.00–2.03 Å.
[g] Molecular replacement (MR) method was used (44).
[h] This number was obtained after SAD phasing before density modification (40).

TABLE 2
Results of docking to KinB-SD for potential signaling molecules

Compound	Mannose 6-phosphate	Glucose 1-phosphate	Fructose 6-phosphate	Mannose 1-phosphate	Glucose 6-phosphate
FRED Chemgauss 4 Score	−10.96	−9.84	−9.78	−9.49	−8.45

The data were analyzed using the program GraphPad Prism mentioned earlier.

Dynamic Light Scattering Assay—Dynamic light scattering (DLS) was performed using DynaPro Plate Reader Plus (Wyatt Technologies, Inc.) in a 384-microwell plate format. The experiment was to measure the hydrodynamic radius of the KinB-SD and its evolution during a heating ramp in the presence and absence of small ligands. An increase of the hydrodynamic radius of a protein with a temperature is an indication of protein thermal denaturation and subsequent aggregation (45). A shift of the temperature in the presence of a potential ligand suggests an influence of the ligand on the thermal stability/unfolding/aggregation of the protein. Typically, the molecular hydrodynamic radius does not necessarily reach a plateau during heating, and the measurement of the hydrodynamic radius of the protein tends to fluctuate after a protein starts to unfold and aggregate; a melting temperature cannot be simply defined based on a given fitting model, such as the calculated peak position of the first derivation of the melting curve using a Gaussian distribution model. Therefore, the onset of the hydrodynamic radius expansion was defined as a characteristic temperature (T_{onset}) when the calculated first derivative reaches 1, which approximately means that the hydrodynamic radius doubles its size per degree Kelvin at the temperature. The radius usually rapidly becomes larger after this point. Before the calculation of the first derivative values, melting curves were subjected to a 5-point unweighted smoothing using GraphPad Prism.

In Silico Ligand Screening—To investigate potential signaling molecules, a geometric representation of the cavity formed at the KinB-SD dimer interface was virtually screened against a library of known binding pockets extracted from the Protein Data Bank (PDB) (46). Comparing the shape and physicochemical composition of the KinB-SD pocket, a set of ligands was identified that adhere to the geometric and biochemical constraints of the pocket. Reducing this set by filtering for a phosphate group, a list of potential signaling molecules was obtained (Table 2). The molecules were docked using the software FRED (OpenEye Scientific). During docking, all conformations of the molecules were iterated to identify a consensus pose. Two independent runs were conducted, one in which the bound phos-

phate was used as a constraint to pose the molecules and one where the molecules were able to explore all possible conformational spaces. Both iterations provided the same final pose. The Chemgauss 4 scores for each molecule are shown in Table 2.

Ligand Binding Using Biolayer Interferometry—BLI was used to measure the interaction of the KinB-SD with the top two ligands predicted by *in silico* analysis and involved in alginate synthesis. The KinB-SD with an avi tag was purified as described earlier. Assays were performed in 96-well black microplates (Fisher) at 30 °C on an Octet RED instrument (*Forté*BIO). The KinB-SD was loaded onto Super Streptavidin biosensors (*Forté*BIO) at a concentration of 2 mg/ml in phosphate-buffered saline (PBS) buffer. The reference Super Streptavidin biosensors were blocked with EZ-link biocytin (Thermo Scientific) at 10 μg/ml in PBS buffer. For comparison, both sugars and their phosphorylated derivatives were tested. Each sugar was titrated from 0.23 to 30 mM in a buffer containing 20 mM Tris, pH 8.0, 50 mM NaCl, and 2 mM DTT. Triplicate samples were prepared for each sugar dilution. Assays were run first using the protein biosensors, followed by the reference biosensors using the same protocol. The reference data were then subtracted from the protein data to account for nonspecific binding. No binding to the KinB-SD was observed for fructose and mannose. To better estimate binding affinity for the phosphorylated sugars, an expanded concentration range was tested for Man-6-P (0.23–266 mM) and Fru-6-P (0.23–658 mM) with the highest values being near the solubility limit for the examined sugar. To determine apparent equilibrium dissociation constants (K_D), the response signal at equilibrium was plotted against sugar concentration. Steady-state analysis of the data were performed using GraphPad Prism.

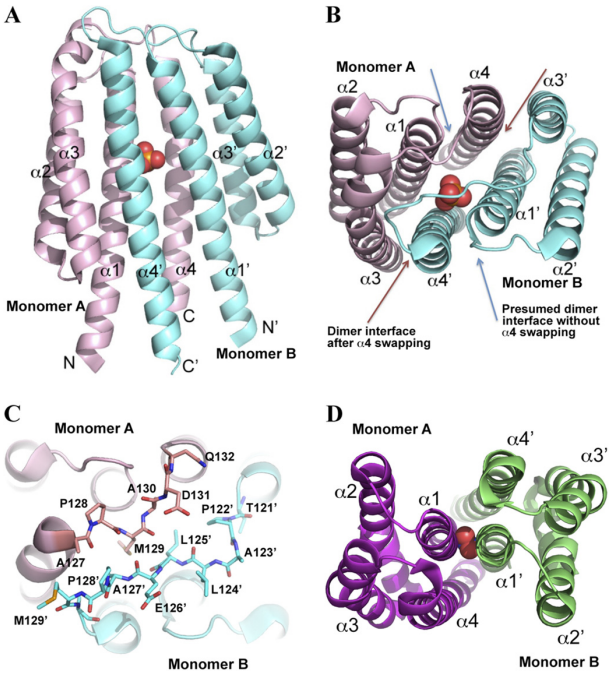

FIGURE 1. **Structure of the helix-swapped KinB-SD dimer.** *A, side view* of a *ribbon* drawing of the KinB-SD dimer. Monomers A and B are colored in *salmon* and *cyan*, respectively. A bound phosphate group is located in a cavity on the SD dimer interface and is drawn as *spheres*. *Primes* on secondary structure labels refer to those from monomer B. *B, top view* of the same *ribbon* drawing as in *A*, showing the asymmetry of the phosphate group binding. The α4 helix is being swapped to increase the dimer interface. *C, stick* drawing of the two α3_α4 loops at the top of the SD dimer, showing their difference in length and conformation. *Primes* on amino acid residue labels refer to those from monomer B. *D, top view* of a *ribbon* drawing of the SD of HK NarX (PDB code 3EZH), showing a typical four-helix bundle dimer. A bound nitrate ion within the dimer interface is drawn in spheres. Figs. 1, 3, 4, 5, *B* and *C*, and 7 were prepared with the program PyMOL.

RESULTS AND DISCUSSION

KinB-SD Forms a Helix-swapped Dimer—The recombinant KinB-SD crystallized under several conditions. We have determined high resolution structures of the ligand-free and phosphate-bound forms (Table 1). In the ligand-free structure, there are eight monomers in one asymmetric unit. The phosphate group-bound structure was determined using a crystal obtained from a crystallization solution containing 2.1 M phosphate; there are two monomers in one asymmetric unit. The ligand-bound form is more structurally ordered and is used below to describe details of the KinB-SD.

In the phosphate-bound structure, two all-helical KinB-SDs form an α4 swapped dimer with an approximate 2-fold symmetry (Fig. 1, *A* and *B*). Monomer A includes residues from Gln-42 to Ala-164 and monomer B from Gln-42 to His-166. In both monomers, the N-terminal SNA sequence (cloning artifact) is visible in the electron density, and it extends the N-terminal α1 helix. Each monomer is composed of four helices with its fourth helix (α4) exchanged in position with the α4′ helix of its partner, creating an eight-stranded α-helical bundle. The two hinge loops between the α3 and α4 and α3′ and α4′ helices, involved in the α4 swapping, are well ordered, and their electron densities are unambiguous in the high resolution structure. However, the hinge loop conformation is very different in the two monomers (Figs. 1, *B* and *C*, and 2*A*). In monomer A, this loop is short (Ala-127 to Asn-132), but in monomer B it is four res-

TABLE 3

Interface properties of swapped and presumably unswapped dimers

The data in the table was calculated using the PISA server. CSS is complexation significance score; N_{HB} is number of potential hydrogen bonds across the interface; N_{SB} is number of potential salt bridges across the interface.

	$N_{residues}$	Interface area	ΔG	ΔG	N_{HB}	N_{SB}	CSS
		Å²	*kcal/mol*	*p value*			
Swapped dimer (open interface)	59	2357.4	−53.3	0.001	9	0	1.00
Swapped dimer without hinge loop[a] (open interface)	52	2075.5	−47.3	0.001	8	0	1.00
Closed monomer without hinge loop[a] (closed interface)	20	1010.0	−24.1	0.022	2	0	1.00
Presumably unswapped dimer without hinge loop[a]	30	1287.8	−5.6	0.397	20	10	0.00

[a] To remove the conformational variation of the hinge loop (Ala-123 to Asp-131), the loop was eliminated for the comparisons. The hinge loop has a minor contribution to the formation of the swapped dimer.

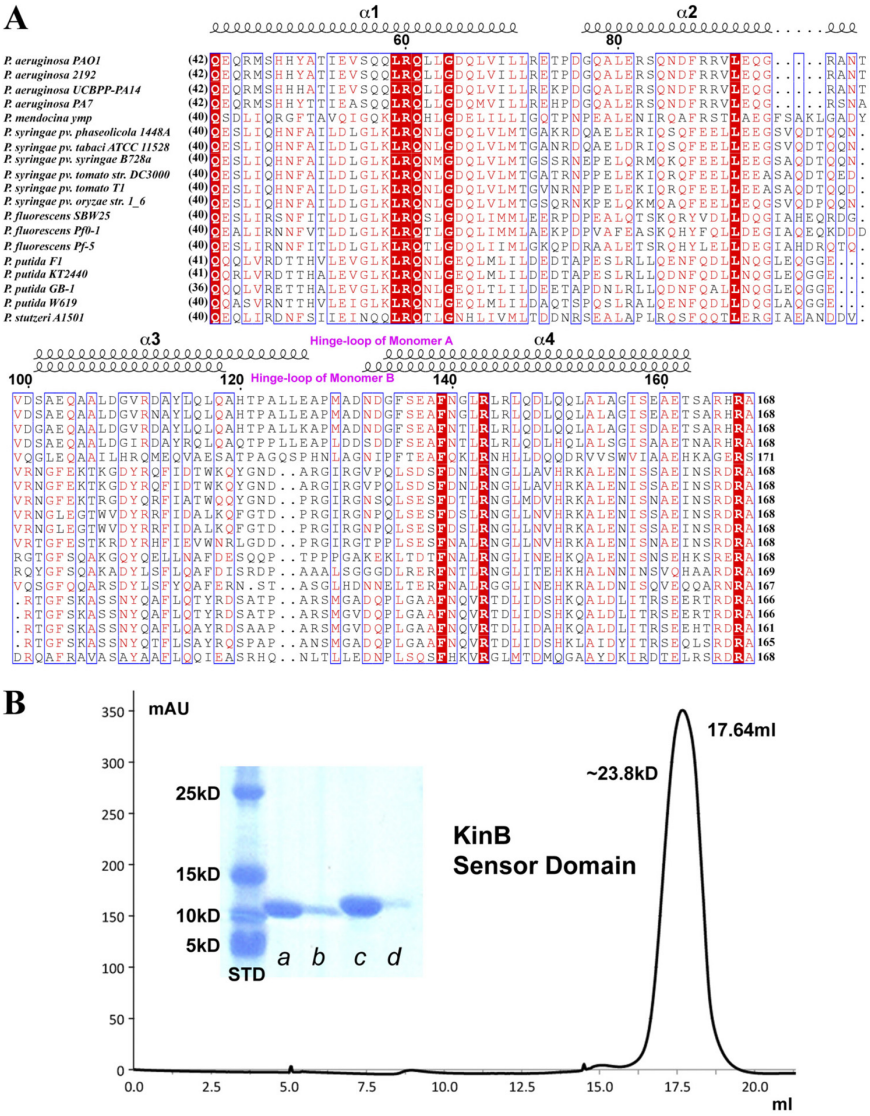

FIGURE 2. **Multiple sequence alignment and size exclusion chromatography of KinB-SD.** *A,* multiple sequence alignment of the SDs of KinB from members of the *Pseudomonas* genus. The α-helices are marked with *coils* above the appropriate sequences. Identical residues are highlighted in *red*. Within the different strains of *P. aeruginosa*, the sequence identities are larger than 85%. The sequence identity with other members of the *Pseudomonas* genus is between 28 and 35%. The sequences used in the alignment include the following: KinB-SDs from *P. aeruginosa PAO1* (gi:15600677); *P. aeruginosa 2192* (gi:254243036); *P. aeruginosa UCBPP-PA14* (gi:116053634); *P. aeruginosa PA7* (gi:152983809); *P. mendocina ymp* (gi:146305216); *P. syringae* pv. *phaseolicola 1448A* (gi: 71733915); *P. syringae* pv. *tabaci ATCC 11528* (gi: 257481808); *P. syringae* pv. *syringae B728a* (gi:66043534); *P. syringae* pv. *tomato* strain DC3000 (gi: 28867566); *P. syringae* pv. *tomato T1* (gi:213971024); *P. syringae* pv. *oryzae* strain 1_6 (gi:237797951); *P. fluorescens SBW25* (gi:229587665); *P. fluorescens Pf0-1* (gi:77456275); *P. fluorescens Pf-5* (gi:70733602); *P. putida F1* (gi:148545406); *P. putida KT2440* (gi:26986877); *P. putida GB-1* (gi:167031168); *P. putida W619* (gi:170724253); and *P. stutzeri A1501* (gi:146284366). The alignment was generated with the programs MultAlin (58) and ESPript (59). *B,* size exclusion chromatography of KinB-SD. Purification of the KinB-SD (Gln-42 to Ala-168) on a Superdex 200 10/300GL column produces a single peak corresponding to a molecular mass of 23.8 kDa, consistent with that of a dimer. The *inset* shows SDS-PAGE of two purified constructs of KinB-SD *Lanes a* and *b* contain two different concentrations of a truncated SD (Arg-45 to Glu-161). No diffraction quality crystals were obtained from this construct. *Lanes c* and *d* contain two different concentrations of the complete SD (Gln-42 to Ala-168) presented in this report. Both constructs migrate on the gel with the apparent molecular mass of about 13 kDa. *mAU*, milliabsorbance units.

idues longer (Thr-121 to Ala-130). The longer loop in monomer B is a result of unwinding of the C terminus of the α3 helix. The two hinge loops show distinct conformations. Particularly, the Met-129 residue in monomer A points inward and is completely buried. The same residue in monomer B is fully solvent-exposed (Fig. 1*C*). When the two monomers are superimposed (using Cα atoms) by least squares (LS) fitting, the resulting root mean square deviation (r.m.s.d.) value is 1.71 Å, and the hinge loops and their proximity show the largest differences.

In a typical four-helix bundle, the α4 helix would make the majority of contact with the α1 and α3 helices of the same chain and in its dimeric form it would interact with two helices, α1′ and α4′, of the second chain (Fig. 1*D*). In the KinB-SD swapped four-helix bundle dimer, the α4 helix interacts only with the α1

helix of the same chain and with three helices, α3′,α1′, and α4′, of the opposite chain. Therefore, because of swapping, the dimer interface now involves three helices (α1, α3, and α4) from each monomer instead of two (α1 and α4) (Fig. 1*B*). The α4-swapping nearly doubles the surface of the dimer interface as compared with the unswapped dimer (Table 3). The total buried surface-accessible area of the α4-swapped dimer is 4714 Å^2 with a complexation significance score of 1 (Table 3) (47). The size exclusion chromatography data (Fig. 2*B*) also indicate that in solution the wild-type KinB-SD exists as a dimer.

A Cavity within the Dimer Interface—The KinB-SD dimer interface shows several distinctive features. In the eight-helix bundle dimer, four helices (α1, α4, α1′, and α4′) are longer and protrude away. Two N and two C termini are located in close proximity (12–16 Å apart) on the same side (Fig. 1*A, bottom*) of the dimer. In the full-length protein, these helices are presumed to extend into the membrane, and therefore this region is proximal to the membrane. On the opposite side of the dimer (Fig. 1*A, top*), the hinge loop-containing region is most distal from the membrane. In the dimer α-helical bundle, there are eight discrete layers of side chain interactions. Six layers of the side chain packing involve all eight helices, and two layers involve only the four longest helices (α1, α4, α1′, and α4′). These interactions involve intra- and inter-monomers. As expected, the majority of interactions are hydrophobic or comprise hydrogen bond networks by highly conserved residues and solvent molecules.

The fifth layer of the KinB-SD shows quite a unique interaction, and it includes strictly conserved Arg-60 residues from helix α1/α1′ on the dimer interface. The planar guanidinium groups of the Arg-60/Arg-60′ side chains from the two opposing monomers are stacked in an almost perfectly parallel fashion with their C^{ζ}–C^{ζ} interatomic distance of 3.68 Å (Fig. 3, *A* and *B*). Stacking of guanidinium moieties of arginine pairs has been reported previously and is quite common in proteins (48). For example, a similar guanidinium-guanidinium ion pair (Arg-3/Arg-89) is present in tryptophan synthase from *Salmonella typhimurium*. This interaction is stabilized by an aspartic acid carboxylate (PDB entry 1KFC) (49). However, this pair as well as many others reported previously are exposed toward the solvent region instead of being buried in the core of the protein (48). Solvent molecules surrounding such an ion pair are believed to provide additional stabilization to the close face-to-face approach of two arginines (50). In the KinB-SD, the energetically unfavorable packing of two positively charged Arg-60 residues at the dimer interface seems mitigated by the local environment. Multiple hydrogen bonds, both direct and water-mediated, between these two arginines and the glutamine residues (including Gln-147/Gln-147′ from the fifth layer, and Gln-57 and Gln-157, from both monomers that form the fourth layer of interaction just below the arginines (not shown in Fig. 3, *A* and *B*)) may help reduce the repelling force between the two guanidinium groups. Nevertheless, this site may be well suited to accept a negatively charged ion.

Above the positively charged fifth layer is the sixth layer that features strictly conserved Gly-64 and Arg-143 and conserved Asp/Glu/Asn-65 (Fig. 2*A*). In this layer, the side chains of the two Arg-143 residues pull away from the center and point outward, forming salt bridges with the Asp-65 residues (Fig. 3, *A* and *B*). The Arg-143 residues are also contacting hydrophobic residues in the seventh layer. If the side chains of these arginines would assume conformation similar to the two Arg-60 residues, the guanidinium groups of Arg-143 residues would have approached each other and positioned exactly above the two Arg-60 guanidinium groups in the fifth layer described earlier, forming a highly unusual cluster of four guanidinium groups at the center of the dimer interface. It appears that Asp-65 serves as a guide for Arg-143 side chain conformation and forces it to bend away and consequently create a cavity on the dimer interface of a volume of 1009.6 Å^3 in the middle of the sixth layer of the helical bundle (Fig. 3, *B* and *C*). The cavity spans across an approximate 2-fold axis that relates the A and B monomers. The core of the seventh layer includes Leu-67 and Phe-139, which seemingly provide a hydrophobic cap for the cavity centered in the sixth layer. Most of the residues that are critical in forming the cavity, including Arg-60, Gly-64, Phe-139, and Arg-143, are completely conserved in KinB HKs within the *Pseudomonas* genus (Fig. 2*A*). This is the only cavity in the KinB-SD that can accommodate a 200–300-Da ligand, and we propose that the cavity serves as the signal molecule-binding site.

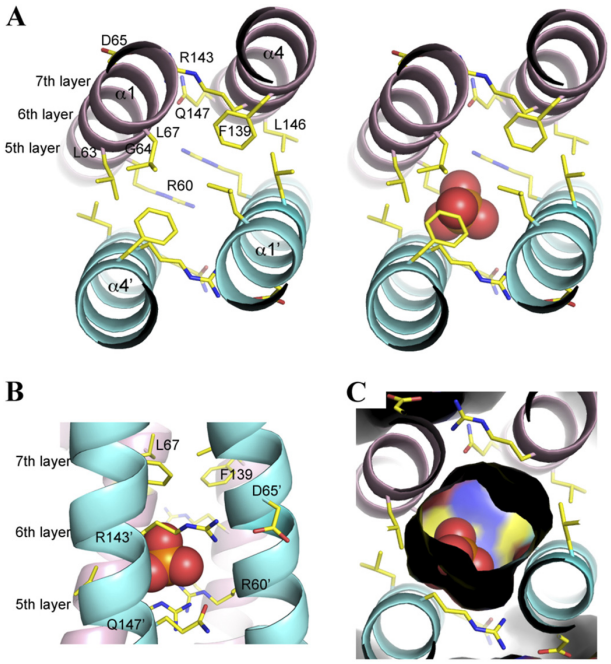

FIGURE 3. **Ligand-binding cavity formed on the dimer interface and the asymmetric binding of a phosphate anion.** *A, top view* of the cavity at the KinB-SD dimer interface with the phosphate removed (*left*) and with the anion present (*right*). *Primes* on secondary structure or amino acid residue labels refer to those from monomer B. The cavity is lined up with residues mainly from the α1/α1′- and α4/α4′-helices drawn in *stick* format. They are part of the fifth, sixth, and seventh layers of side chain interactions in the four-helix bundle dimer. For clarity, only residues from monomer A are labeled for this nearly 2-fold symmetric dimer in *A*. *B, side view* of the phosphate positioning in the cavity. *C, top view* of a molecular surface representation of the ligand-binding cavity. The cavity is cross-sectioned from the top to show the phosphate group.

Asymmetric Binding of a Phosphate in Cavity—In the cavity, a phosphate group is positioned asymmetrically (Fig. 3). It

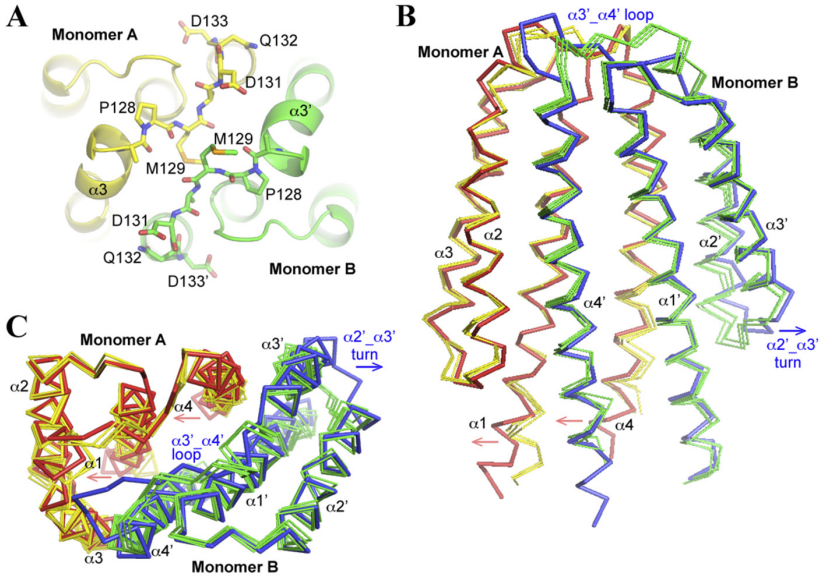

FIGURE 4. **Comparison of the ligand-free and the phosphate-bound four-helix bundle dimer.** *A,* highly symmetric ligand-free SD dimer. The two α3_α4 loops (hinge loop) at the *top* of the ligand-free dimer are similar to each other. Their primary difference is the conformation of residue Met-129, which points inward in monomer A (in *yellow*) and outward in monomer B (in *green*). *Primes* on secondary structure or amino acid residue labels refer to those from monomer B. *B, side view,* and *C, top view* of the superposition of the four ligand-free dimers in one asymmetric unit (all in *yellow* and *green* for monomers A and B, respectively) to the dimer of the phosphate-bound dimer (in *salmon* and *blue* for monomers A and B, respectively). Only monomer A was used in the LS structure fitting. Binding of phosphate appears to induce a major conformational change of the α3_α4 loop and an outward movement of the turn between α2 and α3 (α2_α3 turn) in monomer B. It also induces a tilt of the membrane-proximal parts of the α1 and α4 helices of monomer A.

forms two strong hydrogen bonds with Arg-60 (2.8 and 3.2 Å), one weak interaction with Arg-60′ (3.6 Å), a strong hydrogen bond with main chain carbonyl of Arg-143 (2.8 Å), and a water-mediated hydrogen bond (2.6 Å) that is held by the guanidinium group of Arg-143 and the amino group Gln-147 side chain. There are also several hydrogen bonds to water molecules (not shown in figures) that bridge the anionic group with other surrounding protein atoms. The phosphate group is shifted toward monomer B but makes the strongest interaction with Arg-60 of monomer A. The position of the phosphate group inside the ligand-binding site and the hinge loops are the two most asymmetric elements of the KinB-SD dimer.

Nearly Symmetric Ligand-free KinB-SD—In the ligand-free structure, eight monomers form four similar helix-swapped dimers in one asymmetric unit, which are packed in an alternative up-and-down fashion. In the cavity of each dimer, only water molecules are found. When compared with the phosphate-bound SD, the ligand-free structure has higher atomic displacement parameters (*B*-factors), although its crystal has lower solvent content and a higher diffraction limit. This suggests higher plasticity of the ligand-free KinB-SD dimer (Table 1) and, as often observed, the binding of a phosphate orders the structure.

In each of the four ligand-free swapped dimers, two monomers are more similar to each other and therefore the dimer is more symmetric (pseudo 2-fold) than that in the phosphate-bound dimer. The orientation of Met-129, which points inward in monomer A and outward in monomer B, seems to be the only major difference between the two monomers (Fig. 4*A*). The r.m.s.d. values of the pairwise structural alignment (LS fitting, Cα atoms) of the monomers between the four A-chain monomers (6 pairs), between the four B-chain monomers (6 pairs), and between the A- and B-chains (16 pairs) are 0.67 ± 0.22, 0.35 ± 0.05, and 0.74 ± 0.17 Å, respectively. None of the individual r.m.s.d. values are larger than 1 Å. This is in contrast to the r.m.s.d. value (r.m.s.d. 1.71 Å) from the LS alignment between the chain A and B monomers in the phosphate-bound structure.

The comparison of the phosphate-bound dimer structure with the four ligand-free dimers shows conformational changes induced by phosphate binding (Fig. 4, *B* and *C*). In addition to the large conformational change of the monomer B hinge loop (α3_α4 loop), the phosphate-bound dimer also shows an outward movement of its α2_α3 turn (Fig. 4, *B* and *C*). Most interestingly, in monomer A, the N-terminal portion of α1 and the C-terminal region of the α4 helices shift away from the dimer interface (Fig. 4, *B* and *C*). As indicated earlier, this region is proximal to the membrane, and this shift when propagated across the membrane may change the relative orientation of the HK cytoplasmic domains.

Structures and Dimerization of R60A, R60L, and R60E Point Mutants—Arginine 60 is one of the highly conserved residues of KinB (Fig. 2*A*); it forms a unique symmetrically stacked guanidinium interaction buried on the dimer interface and binds the phosphate anion. To test the structural and functional roles of Arg-60, three point mutations, R60A, R60L, and R60E, were produced and characterized. These mutants, when compared with the wild type, shift the oligomeric state of the KinB-SD in solution from a dimer to a monomer (Fig. 5*A*). In addition, diffraction quality crystals of the R60L and R60E mutants were obtained, and their structures were determined. In solution, R60L is a mixture of monomer and dimer in a ratio of ~2:1.

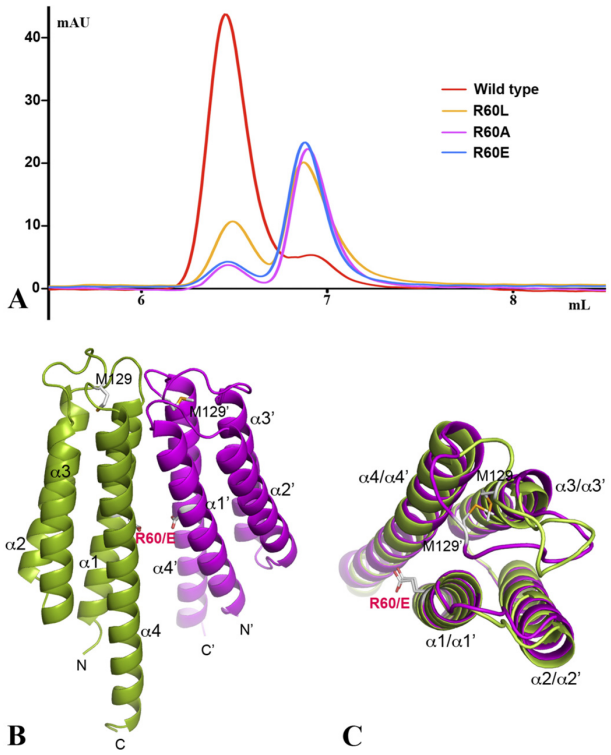

FIGURE 5. **Properties of R60A, R60L, and R60E point mutants.** *A*, size exclusion chromatography of the KinB wild-type (Gln-42 to Ala-168) and its three mutants. The predominant species of the wild-type is dimeric. R60L is a mixture of monomer and dimer. R60A and R60E are mainly monomers in solution. *B*, ribbon drawing of the KinB mutant, R60E. Two monomers in one asymmetric unit are colored in *dark green* and *magenta*, respectively. The monomers form a typical four-helix bundle. The position of the R60E mutation in the structure is highlighted in *stick format*. *C*, superposition of two R60E monomers. The α3_α4 hinge loop is the only region that is structurally different in these structures. *mAU*, milliabsorbance units.

However, the dimeric form of R60L selectively crystallized and shows a structure similar to the more symmetric ligand-free wild-type KinB-SD structure (data not shown). The r.m.s.d. values of the pairwise alignment (LS fitting, Cα atoms) of the monomers from these two structures are 0.88 ± 0.19 Å (24 pairs). This suggests that a substitution of Arg-60 with the amino acid corresponding to the aliphatic part of the arginine side chain but not having a guanidinium moiety can be accommodated on the KinB-SD swapped dimer interface. It appears that a pair of stacked guanidinium groups is not essential for formation of a dimer. However, Arg-60 may be essential for binding of the signaling molecule(s). The R60A and R60E mutants are mostly monomeric in solution. We were able to crystallize the R60E mutant, and it is a monomer in the crystal (Table 1 and Fig. 5). This result is expected because having a pair of glutamic acids with their negatively charged carboxylates pointing at each other is certainly highly unfavorable for a KinB-SD dimer. Several other residues may need to be changed to provide an environment to accommodate buried carboxylates. It is rather surprising that the R60A mutant shows a virtually identical equilibrium between the monomer and dimer as does R60E (Fig. 5*A*). The R60E monomer structure represents a typical four-helix bundle (Fig. 5*B*). In the α4/α4′ helix-swapped dimer, arginine 60 is buried at the dimer interface, whereas in the R60E mutant the glutamate side chain is solvent-exposed. There are two R60E monomers in one asymmetric unit, which are very similar except for the α3_α4 hinge loop region (Fig. 5*C*) and can be superimposed with an r.m.s.d. of 0.62 Å (Ca atoms). The structures of both the R60L and R60E mutants show *B*-factors even higher than the ligand-free wild-type protein (Table 1), underscoring the higher flexibility of the ligand-free structure.

Structural Homologues—A Dali structural homology search (51) using a structure of the helix-swapped monomer form (monomer A) results in no significant hits. The closest match is a three-helix bundle of a spectrin repeat of plectin that aligns with the α1, α2, and α3 helices of monomer A (PDB entry 2ODV, Z-score 8.5, r.m.s.d. value of 2.0 Å, and length of alignment of 87 amino acids with a sequence identity of 7%). The low structural homology of the KinB-SD to protein structures underscores the novelty of the helix-swapped four-helix bundle dimer. In contrast, using the R60E mutant monomer structure as a search template yields a large number of hits. This is not surprising because a four-helix bundle exists as a common structural motif in many protein structures, either as part of a core structure or at protein-protein interfaces (52). Three helix bundle SDs with known structures, TAR (53), NarX (25), and TorS (26), are all among the top hits. For example, the SD of *E. coli* HK NarX has a Z score of 11.5 (PDB entry 3EZH, r.m.s.d. value of 2.5 Å, and length of alignment of 107 amino acids with a sequence identity of 11%).

Binding of a Phosphate Group in Solution—We carried out DSF and CD assays (54) to investigate the binding of a phosphate in solution to the KinB-SD. The protein unfolding temperature (T_m) was measured using DSF at different phosphate concentrations. The T_m gradually shifts to a higher temperature from 47 to 54 °C as the phosphate concentration increases from 0.1 to 1 M (Fig. 6, *A* and *B*). A similar stabilization effect was observed in the pH range of 4.2 to 7.5. However, it appears that the affinity for the phosphate anion is low. CD spectra were also recorded to measure the thermal denaturation of the KinB-SD (Fig. 6*C*). These spectra, based on the measurement of the helical content of the SD, correlate helix unfolding to the thermal denaturation of this all-helical protein. The first derivatives of the unfolding curves of the KinB-SD fits a single Gaussian distribution (Fig. 6, *D* and *E*), suggesting that the unfolding of the SD dimer is largely a one-step event. We also observed an increased T_m at a high phosphate concentration in good agreement with the results of the DSF assay. It suggests that the phosphate ligand bound in the KinB-SD stabilizes the structure and may be a part of a signaling molecule.

Potential Identity and Structural Impact of Signaling Molecule(s)—The nature of the KinB signaling molecule(s) remains unknown, although the KinB-AlgB TCS has drawn noteworthy interests. *In silico* ligand screening was performed to provide a rationale for the exploration of potential ligands based on the cavity properties of the KinB-SD dimer. Surprisingly, the top hits of the docking experiment are monophosphate sugars (Table 2 and Fig. 7), including the precursor and the intermediate of alginate biosynthesis (55), which the KinB-AlgB TCS negatively regulates. These ligands show orientations

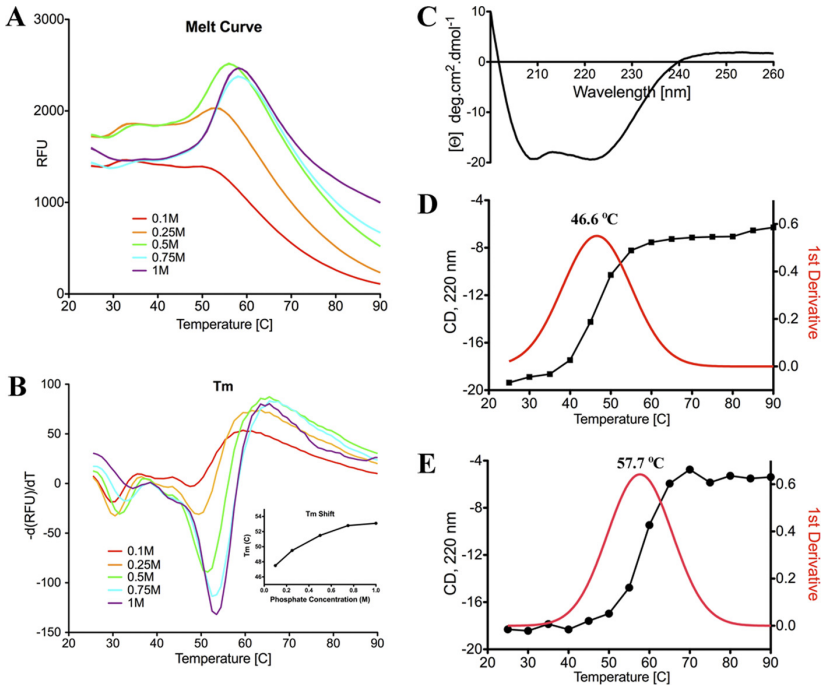

FIGURE 6. **DSF and CD assays.** *A,* DSF assay melting curves for the KinB-SD performed in buffers containing different concentrations of phosphate. The assay was performed at pH 4.2. *RFU,* relative fluorescence units. *B,* the DSF first negative derivative of fluorescence intensity is plotted *versus* temperature. The melting temperature (T_m) is defined as the inflection point of the melting curve, corresponding to the peak of the first negative derivative of the curve. A shift in the T_m indicates a change in protein thermal stability. A decrease in the T_m suggests a destabilization, and an increase in the T_m is interpreted as an increase in protein stability. *C,* CD spectrum of the KinB-SD in Tris buffer (0.1 M Tris, pH 7, 0.15 M NaCl) measured between the wavelengths of 200 and 260 nm at room temperature. It shows a typical profile of an all-helical structure. *D,* CD spectrum was measured at the wavelength of 220 nm as a function of the temperature from 25 to 90 °C in the same Tris buffer as in *C*. *E,* CD spectrum was measured at the wavelength of 220 nm as a function of the temperature from 25 to 90 °C in the Tris buffer as in *C* plus 1 M phosphate buffer (pH 4.2). The *red curve* in *D* and *E* is the Gaussian fitting of the first derivative of each melting curve (*black*). The melting temperatures in both buffers are estimated to be 46.6 ± 0.4 and 57.7 ± 0.3 °C, respectively. The widths of the two distributions are 8.5 ± 0.4 and 8.0 ± 0.3 °C, respectively.

with a nearly identical overlap of the phosphate moiety position in the cavity. To test these results experimentally, binding of precursor Fru-6-P and intermediate Man-6-P of alginate biosynthesis was examined using DSF, CD, and BLI assays. In contrast with the phosphate binding experiments, no significant T_m shift for the KinB-SD could be detected in the presence of these monophosphate sugars using DSF and CD assays (Fig. 6).

However, we were able to estimate binding affinity of Man-6-P and Fru-6-P toward KinB using BLI and an Octet RED system (Fig. 7*B*). For Man-6-P, the estimated equilibrium dissociation constant, K_D was 25 ± 3 mM. It was more difficult to measure the K_D value for Fru-6-P due to solubility limits and instrument limitations, but it was estimated to be ~250 mM. Importantly, the nonphosphorylated analogues (fructose and mannose) were also tested and did not show any binding to the KinB-SD. These results when combined with the phosphate stabilization effect on the KinB-SD suggest that the phosphate group plays an important role in the binding of these monophosphate sugars to the KinB-SD, although overall binding affinities are weak. The apparent K_D value for Fru-6-P is so low that it may be nonspecific. Interestingly, DLS data show that the binding of monophosphate sugars, particularly Man-6-P, destabilizes the KinB-SD structure, resulting in the increase of the hydrodynamic radius of the SD at lower temperatures (Fig. 7*C*). These data confirm the interaction of the KinB-SD with monophosphate sugars, which induces some unfavorable conformational changes and thus decreases the structural stability of the KinB-SD dimer. We attempted to determine structures of KinB-SD complexes with phosphorylated sugars, but thus far co-crystallization with these ligands did not produce crystals containing a bound monophosphate sugar.

The impact of signal molecule binding on the structure and stability of the SD has been rarely studied (23). To produce a conformational change, the binding of a signal molecule may induce the formation of an energetically favorable SD dimer or stabilize a weak SD dimer. However, binding of a signal molecule may disrupt an SD dimer or lower its stability. Both protein thermal stabilization and destabilization by bound ligands have been observed and examined (56). The binding of monophosphate sugars to the KinB-SD may be an example of the latter case, as observed in our DLS experiments. The binding may induce a conformational change in the KinB-SD dimer, reducing its stability; this change is then propagated through the membrane.

A closer inspection of the KinB-SD structure (Fig. 3) and the docking model (Fig. 7*A*) reveals the extensive potential for binding of a phosphate anion-containing sugar molecule that can form hydrogen bonds and hydrophobic interaction in addition to the ionic ones observed for the phosphate anion-Arg-60 (Figs. 2 and 7). However, the lack of hydrogen bonds from the

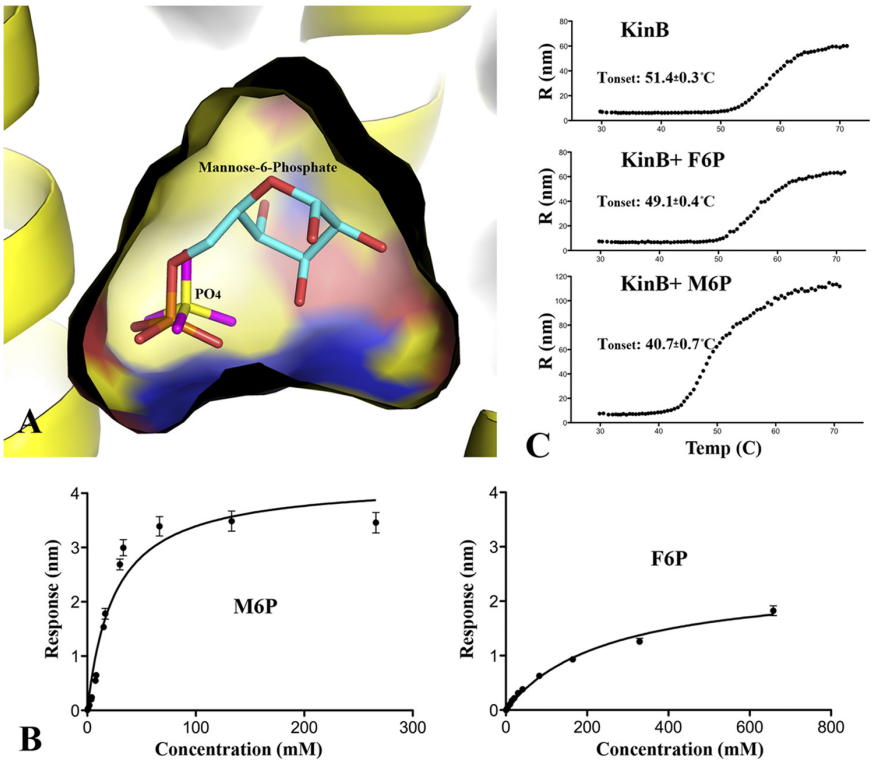

FIGURE 7. **Predicted monophosphate sugars and their interactions with KinB-SD.** *A,* docking of a possible signaling molecule in the binding cavity of the KinB-SD. The top hits of a virtual ligand screening of KinB's presumed signaling molecule(s)-binding site include several monophosphate sugars (Table 3). The figure shows the docking mode of Man-6-P (oxygen atoms in *red*). The position of its phosphate group is similar to the position of the phosphate group (oxygen atoms in *magenta*) found in the phosphate-bound structure. *B,* biolayer interferometry analysis of real time Man-6-P and Fru-6-P binding to KinB using Octet RED system. Response (nanometers) *versus* sugar concentration (millimolar) was plotted for Man-6-P (*left*) and Fru-6-P (*right*), and steady-state analysis was performed. K_D values of 25 ± 3 and ~250 mM were estimated for Man-6-P and Fru-6-P, respectively. *C,* DLS experiments of KinB and KinB in the presence of Fru-6-P or Man-6-P in low salt conditions (50 mM NaCl, 20 mM Tris, pH 8). The values of T_{onset} of each melting curve is an average of three independent runs. Under high salt conditions (250 mM NaCl, 20 mM HEPES, pH 8), none of the melting curves reached plateaus. The values of T_{onset} are 46.3 °C (KinB), 43.2 °C (KinB + Fru-6-P (*F6P*)), and 41.2 °C (KinB + Man-6-P (*M6P*)), respectively (data not shown).

hydroxyl groups of monophosphate sugars to the protein apparently limits the strength of their binding to the KinB-SD. The actual binding modes of monophosphate sugars may be somewhat different from the ones predicted in *in silico* studies (Fig. 7*A*), in which ligands were docked to a rigid KinB-SD dimer. The KinB-SD dimer with a bound monophosphate sugar within the dimer interface may adopt a slightly more open and less energetically favorable conformation.

Several experiments were performed to characterize the effect of binding of monophosphate sugars on the structure and stability of the KinB-SD. Both DSF and CD measurements showed an increase in KinB-SD stability in the presence of phosphate (Fig. 6) but showed no effect in the presence of sugar monophosphates. In contrast, only DLS showed a destabilization of the KinB-SD in the presence of Man-6-P (and with a smaller effect for Fru-6-P) (Fig. 7*C*). The KinB-SD dimer is an α-helix bundle. It is possible that large changes like helix-to-coil transition observed in CD and changes in fluorescence upon binding of dye to hydrophobic regions of proteins recorded in DSF mask the small effect of a weak ligand binding. Only DLS seems to be able to detect subtle perturbation that results in the hydrodynamic radius expansion.

Implication to Signaling Transduction Mechanism—The binding of a signal molecule and dimerization of the HK-SD are regarded as critical steps for signal transduction across the membrane from the periplasm to the cytoplasm. However, these issues continue to remain controversial, because in many cases the nature of a signal molecule and dimerization state of the SD are difficult to prove. For example, PAS-like sensor domains are monomeric or weakly dimeric in solution (19). Some even appear to be monomers in crystals that are grown from highly concentrated protein solutions (22, 28). The known four-helix bundle SD, NarX (25), forms dimers in the crystal, but no oligomeric states in solutions have been reported. The KinB-SD, existing as a dimer in both structure and solution, seems to form a stable homodimer, presumably benefiting from the helix swapping. In HKs it was shown that transmembrane helices, cytoplasmic HAMP, PAS, and His-Kinase-A domains all form homodimers (14). Therefore, the two periplasmic SDs of an HK dimer are very likely physically close to each other in the periplasm, regardless of whether or not a dimer is formed.

Several mechanisms have been proposed on how a SD dimer transmits a signal across the membrane (13–15). These mechanisms generally propose a small structural change induced by ligand binding that is propagated through the membrane. The conformational changes include a ligand binding-induced asymmetry in the SD dimer (57). In this study, we found that the

KinB-SD forms a stable dimer in solution and in the crystal. A cavity is formed at the dimer interface that is large enough to accommodate a small ligand, and it contains a buried arginine pair that may be well suited to accept a negatively charged anion. In the absence of any ligand, the KinB-SD dimer appears to be a flexible and symmetric structure, but it becomes more rigid and somewhat asymmetric upon the binding of a phosphate anion. The binding of the phosphate occurs in the middle of the molecule, but it seems to cause a tilt of the KinB membrane-proximal α1 N- and α4 C-terminal helices that may be a part of the signaling across the membrane. Conformational changes may be caused by asymmetric binding of a ligand that is negatively charged and binds to positively charged Arg-60 pairs inside the dimer. Although the binding of a phosphate group to the KinB-SD is of low affinity, it is suggestive that the signaling molecule may include a phosphate group such as monophosphate sugars, which have been predicted *in silico* and experimentally evaluated in this study. Although these monophosphate sugars bind KinB-SD with low affinity, they are expected to bind the KinB-SD asymmetrically. In general, monophosphate sugars seem to fit well into the profile of a potential signaling molecule, particularly in consideration of their involvement in the biosynthesis pathway of alginate. It is not clear if their weak binding is the nature of KinB's signal molecule(s) or if there are other high affinity ligand(s) that have not yet been identified.

In this study, we present the unique structures of the KinB-SD and our first attempt to identify signal molecule(s). Because KinB down-regulates alginate biosynthesis, high affinity ligands that destabilize the KinB-SD dimer may serve as drugs that can reduce mucus production. Further verification of the roles of the monophosphate sugars and their signal transduction mechanism is of high priority to be addressed. Considering the complexity of TCSs, we cannot exclude possibilities of other signaling molecule(s) interacting with the KinB-SD.

Acknowledgments—We thank members of the Structural Biology Center at Argonne National Laboratory for their help with data collection at the 19-ID beamline and Kimberly S. Buck for help with cloning. This research used resources of the Argonne Leadership Computing Facility at Argonne National Laboratory, which is supported by the Office of Science of the United States Department of Energy under Contract DE-AC02-06CH11357.

REFERENCES

1. Govan, J. R., and Deretic, V. (1996) Microbial pathogenesis in cystic fibrosis: Mucoid *Pseudomonas aeruginosa* and *Burkholderia cepacia*. *Microbiol. Rev.* **60,** 539–574
2. Deretic, V., Gill, J. F., and Chakrabarty, A. M. (1987) Gene algD coding for GDP mannose dehydrogenase is transcriptionally activated in mucoid *Pseudomonas aeruginosa*. *J. Bacteriol.* **169,** 351–358
3. Martin, D. W., Schurr, M. J., Mudd, M. H., Govan, J. R., Holloway, B. W., and Deretic, V. (1993) Mechanism of conversion to mucoidy in *Pseudomonas aeruginosa* infecting cystic fibrosis patients. *Proc. Natl. Acad. Sci. U.S.A.* **90,** 8377–8381
4. Mathee, K., McPherson, C. J., and Ohman, D. E. (1997) Posttranslational control of the algT (algU)-encoded σ22 for expression of the alginate regulon in *Pseudomonas aeruginosa* and localization of its antagonist proteins MucA and MucB (AlgN). *J. Bacteriol.* **179,** 3711–3720
5. Damron, F. H., Qiu, D., and Yu, H. D. (2009) The *Pseudomonas aeruginosa* sensor kinase KinB negatively controls alginate production through AlgW-dependent MucA proteolysis. *J. Bacteriol.* **191,** 2285–2295
6. Parkinson, J. S., and Kofoid, E. C. (1992) Communication modules in bacterial signaling proteins. *Annu. Rev. Genet.* **26,** 71–112
7. Ma, S., Wozniak, D. J., and Ohman, D. E. (1997) Identification of the histidine protein kinase KinB in *Pseudomonas aeruginosa* and its phosphorylation of the alginate regulator algB. *J. Biol. Chem.* **272,** 17952–17960
8. Gooderham, W. J., and Hancock, R. E. (2009) Regulation of virulence and antibiotic resistance by two-component regulatory systems in *Pseudomonas aeruginosa*. *FEMS Microbiol. Rev.* **33,** 279–294
9. Damron, F. H., Owings, J. P., Okkotsu, Y., Varga, J. J., Schurr, J. R., Goldberg, J. B., Schurr, M. J., and Yu, H. D. (2012) Analysis of the *Pseudomonas aeruginosa* regulon controlled by the sensor kinase KinB and σ factor RpoN. *J. Bacteriol.* **194,** 1317–1330
10. Chand, N. S., and Hung, D. T. (2011) The two-component sensor kinase KinB acts as a non-canonical switch between acute and chronic infection. *Virulence* **2,** 553–558
11. Chand, N. S., Lee, J. S., Clatworthy, A. E., Golas, A. J., Smith, R. S., and Hung, D. T. (2011) The sensor kinase KinB regulates virulence in acute *Pseudomonas aeruginosa* infection. *J. Bacteriol.* **193,** 2989–2999
12. Chand, N. S., Clatworthy, A. E., and Hung, D. T. (2012) The two-component sensor KinB acts as a phosphatase to regulate *Pseudomonas aeruginosa* Virulence. *J. Bacteriol.* **194,** 6537–6547
13. Gao, R., and Stock, A. M. (2009) Biological insights from structures of two-component proteins. *Annu. Rev. Microbiol.* **63,** 133–154
14. Cheung, J., and Hendrickson, W. A. (2010) Sensor domains of two-component regulatory systems. *Curr. Opin. Microbiol.* **13,** 116–123
15. Perry, J., Koteva, K., and Wright, G. (2011) Receptor domains of two-component signal transduction systems. *Mol. Biosyst.* **7,** 1388–1398
16. Reinelt, S., Hofmann, E., Gerharz, T., Bott, M., and Madden, D. R. (2003) The structure of the periplasmic ligand-binding domain of the sensor kinase CitA reveals the first extracellular PAS domain. *J. Biol. Chem.* **278,** 39189–39196
17. Cheung, J., Bingman, C. A., Reyngold, M., Hendrickson, W. A., and Waldburger, C. D. (2008) Crystal structure of a functional dimer of the PhoQ sensor domain. *J. Biol. Chem.* **283,** 13762–13770
18. Cho, U. S., Bader, M. W., Amaya, M. F., Daley, M. E., Klevit, R. E., Miller, S. I., and Xu, W. (2006) Metal bridges between the PhoQ sensor domain and the membrane regulate transmembrane signaling. *J. Mol. Biol.* **356,** 1193–1206
19. Pappalardo, L., Janausch, I. G., Vijayan, V., Zientz, E., Junker, J., Peti, W., Zweckstetter, M., Unden, G., and Griesinger, C. (2003) The NMR structure of the sensory domain of the membranous two-component fumarate sensor (histidine protein kinase) DcuS of *Escherichia coli*. *J. Biol. Chem.* **278,** 39185–39188
20. Neiditch, M. B., Federle, M. J., Miller, S. T., Bassler, B. L., and Hughson, F. M. (2005) Regulation of LuxPQ receptor activity by the quorum-sensing signal autoinducer-2. *Mol. Cell* **18,** 507–518
21. Zhou, Y. F., Nan, B., Nan, J., Ma, Q., Panjikar, S., Liang, Y. H., Wang, Y., and Su, X. D. (2008) C4-dicarboxylates sensing mechanism revealed by the crystal structures of DctB sensor domain. *J. Mol. Biol.* **383,** 49–61
22. Cheung, J., and Hendrickson, W. A. (2008) Crystal structures of C4-dicarboxylate ligand complexes with sensor domains of histidine kinases DcuS and DctB. *J. Biol. Chem.* **283,** 30256–30265
23. Wu, R., Gu, M., Wilton, R., Babnigg, G., Kim, Y., Pokkuluri, P. R., Szurmant, H., Joachimiak, A., and Schiffer, M. (2013) Insight into the sporulation phosphorelay: Crystal structure of the sensor domain of *Bacillus subtilis* histidine kinase, KinD. *Protein Sci.* **22,** 564–576
24. Chang, C., Tesar, C., Gu, M., Babnigg, G., Joachimiak, A., Pokkuluri, P. R., Szurmant, H., and Schiffer, M. (2010) Extracytoplasmic PAS-like domains are common in signal transduction proteins. *J. Bacteriol.* **192,** 1156–1159
25. Cheung, J., and Hendrickson, W. A. (2009) Structural analysis of ligand stimulation of the histidine kinase NarX. *Structure* **17,** 190–201
26. Moore, J. O., and Hendrickson, W. A. (2009) Structural analysis of sensor domains from the TMAO-responsive histidine kinase receptor TorS. *Structure* **17,** 1195–1204
27. Ulrich, L. E., and Zhulin, I. B. (2005) Four-helix bundle: A ubiquitous sensory module in prokaryotic signal transduction. *Bioinformatics* **21,**

Suppl. 3:iii45–48
28. Cheung, J., Le-Khac, M., and Hendrickson, W. A. (2009) Crystal structure of a histidine kinase sensor domain with similarity to periplasmic binding proteins. *Proteins* **77,** 235–241
29. Herrou, J., Bompard, C., Wintjens, R., Dupr, E., Willery, E., Villeret, V., Locht, C., Antoine, R., and Jacob-Dubuisson, F. (2010) Periplasmic domain of the sensor-kinase BvgS reveals a new paradigm for the Venus flytrap mechanism. *Proc. Natl. Acad. Sci. U.S.A.* **107,** 17351–17355
30. Stibitz, S. (2007) in *Bordetella Molecular Biology* (Locht, C., ed) pp. 47–68, Horizon Bioscience, Norfolk, United Kingdom
31. Lowe, E. C., Basl, A., Czjzek, M., Firbank, S. J., and Bolam, D. N. (2012) A scissor blade-like closing mechanism implicated in transmembrane signaling in a Bacteroides hybrid two-component system. *Proc. Natl. Acad. Sci. U.S.A.* **109,** 7298–7303
32. Rocchetta, H. L., Burrows, L. L., and Lam, J. S. (1999) Genetics of O-antigen biosynthesis in *Pseudomonas aeruginosa*. *Microbiol. Mol. Biol. Rev.* **63,** 523–553
33. Van Duyne, G. D., Standaert, R. F., Karplus, P. A., Schreiber, S. L., and Clardy, J. (1993) Atomic structures of the human immunophilin FKBP-12 complexes with FK506 and rapamycin. *J. Mol. Biol.* **229,** 105–124
34. Kim, Y., Dementieva, I., Zhou, M., Wu, R., Lezondra, L., Quartey, P., Joachimiak, G., Korolev, O., Li, H., and Joachimiak, A. (2004) Automation of protein purification for structural genomics. *J. Struct. Funct. Genomics* **5,** 111–118
35. Klock, H. E., and Lesley, S. A. (2009) The polymerase incomplete primer extension (PIPE) method applied to high-throughput cloning and site-directed mutagenesis. *Methods Mol. Biol.* **498,** 91–103
36. Eschenfeldt, W. H., Makowska-Grzyska, M., Stols, L., Donnelly, M. I., Jedrzejczak, R., and Joachimiak, A. (2013) New LIC vectors for production of proteins from genes containing rare codons. *J. Struct. Funct. Genomics* **14,** 135–144
37. Rosenbaum, G., Alkire, R. W., Evans, G., Rotella, F. J., Lazarski, K., Zhang, R. G., Ginell, S. L., Duke, N., Naday, I., Lazarz, J., Molitsky, M. J., Keefe, L., Gonczy, J., Rock, L., Sanishvili, R., Walsh, M. A., Westbrook, E., and Joachimiak, A. (2006) The structural biology center 19ID undulator beamline: facility specifications and protein crystallographic results. *J. Synchrotron Radiat.* **13,** 30–45
38. Minor, W., Cymborowski, M., Otwinowski, Z., and Chruszcz, M. (2006) HKL-3000: the integration of data reduction and structure solution–From diffraction images to an initial model in minutes. *Acta Crystallogr. D Biol. Crystallogr.* **62,** 859–866
39. Schneider, T. R., and Sheldrick, G. M. (2002) Substructure solution with SHELXD. *Acta Crystallogr. D Biol. Crystallogr.* **58,** 1772–1779
40. (1994) The CCP4 suite: programs for protein crystallography. *Acta Crystallogr. D Biol. Crystallogr.* **50,** 760–763
41. Cohen, S. X., Morris, R. J., Fernandez, F. J., Ben Jelloul, M., Kakaris, M., Parthasarathy, V., Lamzin, V. S., Kleywegt, G. J., and Perrakis, A. (2004) Towards complete validated models in the next generation of ARP/wARP. *Acta Crystallogr. D Biol. Crystallogr.* **60,** 2222–2229
42. Emsley, P., and Cowtan, K. (2004) Coot: model-building tools for molecular graphics. *Acta Crystallogr. D Biol. Crystallogr.* **60,** 2126–2132
43. Murshudov, G. N., Vagin, A. A., and Dodson, E. J. (1997) Refinement of macromolecular structures by the maximum-likelihood method. *Acta Crystallogr. D Biol. Crystallogr.* **53,** 240–255
44. Vagin, A., and Teplyakov, A. (2010) Molecular replacement with MOLREP. *Acta Crystallogr. D Biol. Crystallogr.* **66,** 22–25
45. Shiba, K., Niidome, T., Katoh, E., Xiang, H., Han, L., Mori, T., and Katayama, Y. (2010) Polydispersity as a parameter for indicating the thermal stability of proteins by dynamic light scattering. *Anal. Sci.* **26,** 659–663
46. Berman, H. M., Westbrook, J., Feng, Z., Gilliland, G., Bhat, T. N., Weissig, H., Shindyalov, I. N., and Bourne, P. E. (2000) The Protein Data Bank. *Nucleic Acids Res.* **28,** 235–242
47. Krissinel, E., and Henrick, K. (2007) Inference of macromolecular assemblies from crystalline state. *J. Mol. Biol.* **372,** 774–797
48. Lee, D., Lee, J., and Seok, C. (2013) What stabilizes close arginine pairing in proteins? *Phys. Chem. Chem. Phys.* **15,** 5844–5853
49. Kulik, V., Weyand, M., Seidel, R., Niks, D., Arac, D., Dunn, M. F., and Schlichting, I. (2002) On the role of αThr183 in the allosteric regulation and catalytic mechanism of tryptophan synthase. *J. Mol. Biol.* **324,** 677–690
50. Soetens, J.-C., Millot, C., Chipot, C., Jansen, G., J. , Ángyán, J., and Maigret, B. (1997) Effect of polarizability on the potential of mean fluorescence of two cations. The guanidinium-guanidinium ion pair in water. *J. Phys. Chem. B* **101,** 10910–10917
51. Holm, L., and Rosenström, P. (2010) Dali server: conservation mapping in 3D. *Nucleic Acids Res.* **38,** W545–W549
52. Lin, S. L., Tsai, C. J., and Nussinov, R. (1995) A study of four-helix bundles: investigating protein folding via similar architectural motifs in protein cores and in subunit interfaces. *J. Mol. Biol.* **248,** 151–161
53. Milburn, M. V., Privé, G. G., Milligan, D. L., Scott, W. G., Yeh, J., Jancarik, J., Koshland, D. E., Jr., and Kim, S. H. (1991) Three-dimensional structures of the ligand-binding domain of the bacterial aspartate receptor with and without a ligand. *Science* **254,** 1342–1347
54. Nettleship, J. E., Brown, J., Groves, M. R., and Geerlof, A. (2008) Methods for protein characterization by mass spectrometry, thermal shift (ThermoFluor) assay, and multiangle or static light scattering. *Methods Mol. Biol.* **426,** 299–318
55. Pawar, S. N., and Edgar, K. J. (2012) Alginate derivatization: a review of chemistry, properties and applications. *Biomaterials* **33,** 3279–3305
56. Cimmperman, P., Baranauskiene, L., Jachimoviciute, S., Jachno, J., Torresan, J., Michailoviene, V., Matuliene, J., Sereikaite, J., Bumelis, V., and Matulis, D. (2008) A quantitative model of thermal stabilization and destabilization of proteins by ligands. *Biophys. J.* **95,** 3222–3231
57. Neiditch, M. B., Federle, M. J., Pompeani, A. J., Kelly, R. C., Swem, D. L., Jeffrey, P. D., Bassler, B. L., and Hughson, F. M. (2006) Ligand-induced asymmetry in histidine sensor kinase complex regulates quorum sensing. *Cell* **126,** 1095–1108
58. Corpet, F. (1988) Multiple sequence alignment with hierarchical clustering. *Nucleic Acids Res.* **16,** 10881–10890
59. Gouet, P., Courcelle, E., Stuart, D. I., and Métoz, F. (1999) ESPript: analysis of multiple sequence alignments in PostScript. *Bioinformatics* **15,** 305–308